SLAC-PUB-6273
June 1993
(A)

Polarized electron beams for linear colliders*

J. Clendenin
Stanford Linear Accelerator Center
Stanford University, Stanford, CA 94309

Abstract

Longitudinally polarized electron beams for high energy collisions provide a sensitive way to explore the electroweak process as well as an effective means to measure spin dependent properties of particles. Once created, such beams are readily accelerated by linacs without loss of polarization, although emittance damping rings present potential hazards. The essential elements of a collider necessary for the utilization of polarized electrons are described. The key element is the polarized electron source as illustrated by the SLC which now operates with $P_e \sim 80\%$ in the 50 GeV linac. Possible improvements for future colliders are discussed.

1. Introduction

As the search for the ultimate structure of matter exposes new particles, reveals more complexity of structure, and teaches more about the forces that govern all the interactions of matter, ever higher energies are required to explore the new frontiers. Figure 1 shows that for the past several

*Work supported in part by Department of Energy contracts DE–AC03–76SF00515 (SLAC).

Invited talk presented at the Workshop on High Intensity Electron Sources, Legnaro, Padova, Italy, May 24–28, 1993.

decades, accelerator technology has improved sufficiently to permit an order of magnitude increase in the center-of-mass energy about every 12 years. We are now on the doorstep of a new increment in this energy with the advent of new hadron colliders (the LHC and SSC) and new e^+e^- colliders (the NLC and JLC among others proposed). All of the new e^+e^- proposals are for linear accelerators because of the large energy loss due to synchrotron radiation in circular accelerators. Since the synchrotron loss scales inversely with the fourth power of the mass, hadron accelerators are considerably less sensitive to synchrotron losses. A simple illustration of the NLC design is shown in fig. 2. It is basically two linacs that are aimed at each other, each capable of accelerating particles to 250–500 GeV.

Hadron collisions present several nice features for experimental particle physics, including much larger cross sections than for e^+e^- collisions. However e^+e^- colliders have a number of advantages over hadron colliders. Particle identification is considerably easier with e^+e^- collisions since there is a clear separation of annihilation species from other possible processes. In addition, Z– and W–pair production becomes a major part of the annihilation cross section above 100 GeV. For practical considerations in detector design, the lower level of radiation damage and event buildup for luminosities above 10^{33} cm^{-2} s^{-1} is important. Finally, and most relevant to the subject of this discussion, good use can be made of polarized electrons.

The luminosity required for new e^+e^- colliders operating at 1 TeV is driven by the need to produce at least 10^3 events/year for a reaction cross

section of 1 R, where R is the elementary QED point cross section for $e^+e^- \rightarrow \mu^+\mu^-$,

$$1\ R = \frac{4\pi\alpha^2}{3s} = \frac{87}{[E(TeV)]^2}\ fb\ , \qquad (1)$$

where s is the usual square of the center-of-mass energy. This is a relevant scale for pair-produced particles since

$$\sigma(e^+e^- \rightarrow X\bar{X}) = A \cdot (1\ R) \cdot \text{phase space}\ , \qquad (2)$$

and since A varies between 0.25 and 5 for all pair species, including Z and W, if forward and backward peaks are excluded. These considerations lead to a minimum luminosity of 10^{33} cm^{-2} s^{-1} for an e^+e^- collider in the 1 TeV range.

2. Polarization Effects at High Energy [1]

Polarization is an important feature of e^+e^- physics above 100 GeV. Since the weak interactions are essentially handed, all e^+e^- reactions have some dependence on polarization through the interference of virtual γ and virtual Z contributions. Above 100 GeV, these contributions become equal. A sampling of polarization asymmetries is shown in table 1. Notice the particularly large asymmetry for W^+W^- production. The $e^+e^- \rightarrow W^+W^-$ production provides a good handle on Standard Model (SM) backgrounds, which is especially useful in searches for new species. The longitudinal polarization of the relativistic W should be connected in some way to the mechanism of mass generation of the W boson, revealing either composite particles or providing a window on Higgs. The differ-

ential cross sections are shown in fig. 3. The large forward-backward asymmetry for polarized e^- is also apparent.

High-luminosity e^+e^- colliders with a highly polarized e^- beam are particularly useful for determining the error on the mass of the W boson in the SM. Figure 4 illustrates that at the Z° pole, a value can be achieved of

$$\Delta m_W \sim 21 \text{ MeV} \tag{3}$$

with 10^6 Z° events for a polarization of 90% and a polarization accuracy on the order of 2%. Such a measurement is within reach of the SLC in 1994–95.

The top quark has not yet been discovered, but is generally accepted as an established part of the SM. From electroweak radiative corrections, an upper limit on the mass has been established as

$$m_t < 200 \text{ GeV} . \tag{4}$$

Thus the top quark will probably be discovered by one of the existing hadron colliders, such as the Tevatron, but with a precision expected to be only on the order of

$$\Delta m_t \sim 5 \text{ GeV} . \tag{5}$$

As will be discussed later, an uncertainty in m_t of < 1 GeV is needed to specify the mass of the Higgs. Fortunately this can be provided by an e^+e^- collider. As shown in fig. 5, a large polarization asymmetry is expected for the reaction $e^+e^- \rightarrow t\bar{t}$. For the NLC/JLC, one can expect

$$\Delta m_t \sim 0.2 \text{ GeV} . \tag{6}$$

The discussion above of W– and t–pair production is important because of its bearing on the Higgs. Basically, the SM doesn't account for the origin of mass. Rather, the masses of weak bosons, quarks, and leptons arise in the SM from an interaction with Higgs bosons (or some external agent) causing the spontaneous breaking of $SU(2) \times U(1)$ symmetry. The SM allows, but doesn't explain, this mechanism.

Theories of the Higgs mechanism can be divided into three groups: the minimal, the weak-coupling, and the strong-coupling models. The minimal model represents the least extension from the SM and present experimental results. In this model, the Higgs mechanism causes three of the four degrees of freedom of the self-interacting scaler field to be absorbed as longitudinal polarization states of weak bosons. The fourth degree is associated with a proposed neutral Higgs boson (singular) with scalar coupling to matter. Possible reactions that produce H° are shown in fig. 6.

In the SM, the masses of H°, W, and t are interrelated through radiative corrections; an example is shown in fig. 7. Limits on the mass of the Higgs boson are set from the error in the measurement of both m_t and m_W. A plot of the 1-σ contours in the m_H-m_t plane is shown in fig. 8. With the experimental realization of Δm_t and Δm_W discussed above, the bounds on the Higgs mass will be greatly improved.

Present experiments exclude $m_{H^\circ} < 58$ GeV. LEP II will be sensitive up to a mass of $m_{H^\circ} \sim 80$ GeV. Hadron colliders are sensitive in the range $160 < m_{H^\circ} < 700$ GeV, depending on the decay mode. On the other hand, e^+e^- colliders should be sensitive up to 1 TeV unless m_{H° is near m_W or m_{Z°.

The weak-coupling models of the Higgs mechanism use scalar couplings to matter. It results in many new, heavy particles: heavy quarks and leptons, charged Higgs particles, and the full array of SUSY particles. This model includes the possibility of a second Z° particle. A dramatic resonance in $e^{+}e^{-}$ annihilation would be expected at the energy of such a particle. Unfortunately, the exact masses of these particles are difficult to predict. Although some of the superparticles are predicted to have masses <200 GeV, most are expected to be >400 GeV.

The strong-coupling models of the Higgs mechanism are the most difficult to attach to experimental particle physics in the present or near future. The required energies are >1 TeV. The models propose strong interactions which mimic QCD and include technicolor, as well as composite quarks and leptons.

3. Acceleration of Polarized Electrons in Linacs

Due to the anamalous dipole moment of the electron, the spin vector of a longitudinally polarized electron will precess relative to the electron momentum vector when subjected to the dipole magnetic guide fields of a circular machine. Thus, in circular machines, the spin vector is usually maintained perpendicular to the plane of the machine—a feat that is made more difficult when encountering the natural spin-flip resonances of the ring as the energy is ramped. By contrast, a linear accelerator has no known depolarization mechanisms.

The acceleration of longitudinally polarized electrons to high energy was pioneered at SLAC in 1974 in a series of experiments with fixed targets. This first experience was with the pre–SLC 3–km linac. The longitudinally polarized electron beam, with $P_e \sim 85\%$ but very low peak intensities, was produced by a Li atomic beam source. The beamline had a Mott polarimeter at 60 keV and a MØller polarimeter in the target area at ~25 GeV. No depolarization was detected.

In 1977, the first GaAs photocathode polarized electron source for accelerators was introduced at SLAC for a parity violating experiment. The source polarization was only ~40%, but the peak intensities matched the capability of the linac at that time. The lack of any depolarization was confirmed with new Mott and MØller polarimeters. (This source and its Mott polarimeter are still in use in the laboratory for high polarization cathode studies.)

Between 1981 and 1991, there were no polarized beams at SLAC, although polarized beams using GaAs sources were available for varying periods at the 2-GeV synchrotron at Bonn and the Mainz microtron (MAMI). During this period, polarized beams were detected at Tristan, LEP, and DESY, generated internally by the action of synchrotron radiation. (Nothing more will be said in this paper about interal generation of polarized beams.)

In early 1992, the SLC began routine operation with a polarized electron beam. A sketch of the SLC is shown in fig. 9. The SLC polarized beam system consists of a new, high-peak intensity, polarized electron source utilizing a III-V semiconductor photocathode. There is no Mott

detector on the beamline. The required spin manipulation for the damping ring and the e^+e^- interaction region (IR) is provided by three superconducting solenoids, and by closed orbital bumps used in the arcs. The polarization of the beam can be measured at the end of the 50 GeV linac by a MØller polarimeter, and at the IR by a Compton polarimeter.

In 1992, the SLC source used a bulk GaAs cathode operated at room temperature [5]. A charge of 8 nC for the 2 ns pulses as required by the injector was readily produced, but the polarization was only 27% at the source, decreasing to 22% at the IR. The depolarization was identified as ~5% in the damping ring, due to a slight energy mismatch; as ~10% in the arc, due to spin diffusion; but as <1% at the IR. For 1993, the damping ring energy was corrected, reducing the depolarization there to about 2%.

4. Polarimetry [6]

The location of the SLC MØller and Compton polarimeters is shown in fig. 10. MØller scattering is the elastic scattering of polarized e^- from polarized e^-. The Feynman diagrams are shown in fig. 11. The relative phase between the two diagrams is negative. The target electrons are usually provided by a magnetized iron plate inserted into the beam. The unpolarized differential cross section as well as the longitudinal and transverse asymmetry functions are presented in fig. 12 as a function of the center-of-mass scattering angle. Note that at $\theta = 90^\circ$, where the analyzing power is a maximum, the transverse asymmetry is nearly an order of magnitude lower than for longitudinal. A schematic of the SLC MØller polarimeter is shown in fig. 13.

There are at least three advantages of a MØller polarimeter:

(1) the possibility of 3–axis polarimetry—a dubious distinction given the relatively low asymmetry for transverse polarization,

(2) high counting rates, and

(3) large asymmetries A(θ).

The experimental asymmetry, A_{exp}, is given by

$$A_{exp} = P_{target} \cdot P_{beam} \cdot A(\theta) \ . \qquad (7)$$

Unfortunately, the target polarization is quite small, ~8%, so that typically it takes about five minutes to get a polarization measurement for the longitudinal component of the beam with 5% accuracy, while for the transverse component, at least an hour would be required.

Compton scattering is the elastic scattering of polarized e^- from polarized γ. Only left or right circularly-polarized γ are involved, since longitudinally polarized γ produce no asymmetry. The Feynman diagrams for the processes involved are shown in fig. 14. In this case, the relative phase is positive. The Compton cross section can be expressed as

$$\frac{d^2\sigma}{dxd\varphi} = \left(\frac{d^2\sigma}{dxd\varphi}\right)_{unpol} \left\{1 - P^\gamma \left[P_z^e \ A_z^{e\gamma}(x) + \ P_t^e \cos\varphi \ A_z^{e\gamma}(x)\right]\right\} \ , \qquad (8)$$

where $x \equiv K'/K'_{max}$, K' is the scattered photon energy, and φ is the azimuth of the photon with respect to the e^- transverse polarization. The unpolarized cross section, as well as transverse and longitudinal asymmetries, are shown as a function of x in fig. 15. A schematic diagram of a Compton polarimeter is shown in fig. 16.

With Compton polarimetry, the asymmetries for detection of scattered e^- are large at large x, where the backward scattered e^- have the smallest energy, and thus are easiest to separate from the main beam. In addition, the backgrounds are primarily machine related, and are easily measured by not firing the laser. Compton measurements of longitudinal polarization can be made to an accuracy of 1% within a few seconds. On the other hand, it is not practical to measure tranverse polarization by detecting the scattered e^-.

The P_e can also be measured by detecting the scattered γ. The principle motivation might be to allow the measurement of transverse polarization. However, the energy spectrum of the γ is difficult to measure (integrating over all K' reduces the analyzing power), and a transverse polarization measurement would have practical difficulties in any case .

In the SLC, the Compton polarimeter is located in the extraction beamline after the interaction point as shown in fig. 10. During colliding beam runs, the polarization is continuously monitored by analyzing the scattered electrons.

5. Spin Manipulation [6]

The evolution in time of the electron spin vector, $\hat{s}$—together with the equations of motion for an electron with momentum $\vec{p}$ and energy $\mathcal{E}$, in a magnetic field $\vec{B}$ and electric field $\vec{E}$—are given by the following three equations:

$$\frac{d\hat{s}}{dt} = \hat{s} \times \frac{e}{m}\left[\left(\frac{g-2}{2}+\frac{1}{\gamma}\right)\vec{B} - \left(\frac{g-2}{2}\right)\frac{\gamma}{\gamma+1}\left(\vec{\beta}\cdot\vec{B}\right)\vec{\beta} - \left(\frac{g}{2}-\frac{\gamma}{\gamma+1}\right)\vec{\beta}\times\vec{E}\right], \quad (9)$$

$$d\vec{p} = e\left[\vec{E} + \vec{\beta} \times \vec{B}\right] , \tag{10}$$

and

$$\frac{d\hat{\mathcal{E}}}{dt} = e\,\vec{\beta} \cdot \vec{E} \tag{11}$$

There are two cases of interest, relating to transverse and longitudinal polarization respectively. In the case of transverse polarization, $\hat{s} \perp \vec{\beta}$, the motion of the spin vector in a solenoidal field, where $\vec{\beta} \parallel \vec{B}$ is given by

$$\frac{d\hat{s}}{dt} = \hat{s} \times \vec{\omega}_p , \tag{12}$$

where

$$\vec{\omega}_p = \frac{e\vec{\beta}}{m\gamma} \tag{13}$$

is the Lorentz dilated rest frame rotation rate.

For longitudinal polarization $\hat{s} \parallel \vec{\beta}$ in which $\vec{\beta}$ is initially perpendicular to $\vec{B}$ (i.e., for transverse magnetic fields), the precession of $\hat{s}$ relative to $\vec{\beta}$ is given by

$$\Delta\theta = \left(\frac{g-2}{2}\right) \gamma\, \theta_b , \tag{14}$$

where θ_b is the bending angle experienced by the particle and $a \equiv (g-2)/2 \sim 1.16 \times 10^{-3}$ is the anomalous magnetic moment of the electron.

To preserve the polarization in the SLC damping ring, a solenoidal spin rotator is located in the transport line between the linac and the ring at a point given by $\Delta\theta = (n + 1/2)\,\pi$; i.e., at a point where $\hat{s}$ is horizontal with respect to $\vec{\beta}$. The action of the solenoidal field then rotates $\hat{s}$ to be vertical.

In the original SLC design, two solenoidal spin rotators after the damping ring were to rotate the $\hat{s}$ so as to be parallel to $\vec{p}$ at the interaction point, correcting for the effects of the damping-ring-to-linac transport line and the e^- arc between the linac and the IP. However, SLC now operates with flat beams generated by reducing the betatron coupling in each damping ring. Since the solenoids rotate the planes of the beam beta orbits, they cannot now be used after the damping ring. Fortunately, the spin tune of the arcs turned out to be equal to the vertical betatron tune, so that local "bumps" in the betratron orbit in the e^- arc can be used to make the necessary adjustments in the e^- spin vector. Future colliders, not having arcs, will require relatively elaborate optical systems for adjusting the spin vector of a flat beam, using frequent corrections with skew quadrupoles.

6. Polarized Electron Sources

Colliders require polarized electon beams with high longitudinal polarization at the interaction point[7]. To eliminate the effects of drift, the polarization should be reversible on a pulse-to-pulse basis. Since linear colliders are inherently low duty factor machines, the required high luminosity can only be achieved with high peak current densities, as well as small beam sizes at the IP. The latter property depends on achieving a small beam emittance. However, all present collider designs—with the possible exception of TESLA—include emittance damping rings, so that the tranverse and longitudinal emittance requirements of the e^- source are somewhat relaxed. The pulse-to-pulse stability requirements of the source

depend on the damping ring design. Finally, the source must be available for accelerator operations at least 90% of the time.

Photocathode sources utilizing III–V semiconductor photocathodes appear to be the only viable alternative in the forseeable future. The present performance of the SLC polarized electron source illustrates the capabilities of such a technique and also points to the areas where improvements important for future colliders can be made.

Strained-layer photocathodes consisting of a thin layer of MOCVD-grown GaAs on a $GaAs_{(1-x)}P_x$ sublayer have been shown to yield photoelectrons with polarization as high as 90% if produced with circularly polarized light of the proper wavelength [8]. Since the required wavelength is very close to the bandgap threshhold, where the optical absorption coefficient is very small, and since the thickness of the active layer is only a fraction of one optical absorption depth, the resulting low quantum efficiency (QE) as measured at low photon flux necessitates relatively high-energy laser pulses. Additionally, earlier work at SLAC revealed a limit on the charge that will be emitted from a thick GaAs cathode having low QE [9]. For this reason, the initial SLC strained-layer cathode was chosen to be relatively thick, 0.3 μm, for which the maximum polarization had been measured to be about 80% at 855 nm. With the cathode fully illuminated, the maximum photoyield for a QE of ~1% was found to be $\sim 7 \times 10^{10}$ e^- cm^{-2} in the 2 s pulse produced by the SLC source laser.

The SLC source operates with a polarization of ~80%, reversable on a pulse-to-pulse basis using a Pockels cell and cross polarizer [10]. For

normal operation the peak current is maintained at $\sim 5 \times 10^{10}$ e^- per pulse. The YAG-pumped, Q-switched and cavity-dumped Ti:sapphire laser used to excite the photocathode has a nominal intensity stability of about 3% rms when well tuned. The cathode is operated in saturation mode by adjusting the laser spot size on the cathode, resulting in an e^- beam stability of ~1%. The rms position stability of the laser on the 14 mm (diameter) cathode is <50 μm. The availability of the source is >95% and increasing.

The SLC accelerating rf is S-band (2856 MHz), with a period of 350 ps. The gun is designed to operate at 200 kV with a space charge limit of 15 A. Operation to date has been limited to 120 kV. The normalized rms emittance is calculated to be 10 π mm-mrad. The SLC injector design includes two subharmonic rf bunchers that compress the longitudinal phase space to less than 100 ps before the beam enters an S-band buncher and 3-m accelerator section. The tranverse emittance of the beam increases by an order of magnitude in the bunchers. The energy spread of the beam leaving the cathode is small, but due to space charge forces, it increases to a few percent before acceleration.

7. Future Source Development

Although 100% polarization has not actually been achieved, the problem of high polarization has essentially been solved. Higher polarization can be achieved with ultra-thin strained-lattice cathodes, but in some cases one might prefer to trade the very highest polarization for other desirable properties, such as high peak charge or long lifetimes. For

the SLC source, the lifetime and reliability are greatly improved by the use of a load-lock system to introduce a fresh cathode into the gun chamber after baking and HV processing[11]. The peak current of the SLC source is limited by the maximum cathode bias that can be sustained with low dark current. The peak current can be increased by going to a higher bias using pulsed (instead of DC) high voltage and/or by increasing the size of the photocathode.

The charge limit of the GaAs photocathode is still a serious problem. This limits both the charge that can be produced in a single pulse, and also affects the charge in subsequent closely spaced pulses. Methods to reduce this effect need to be developed.

Source lasers continue to need improvement. With the advent of tunable Ti:sapphire lasers, one can produce the needed high-energy pulses at the correct wavelength, but stability and reliability issues remain. Some improvement is expected if the present flashlamp-pumped Nd:YAG lasers used to pump the Ti:sapphire rods can be replaced with diode-pumped Nd: YAG lasers.

8. Low Emittance Sources

The possibility of developing a very low emittance source of polarized electrons has obvious applications for linear colliders, including simplification of the e^- injection system and possibly the elimination, or at least the simplification, of the e^- damping ring [12]. An rf gun is an obvious candidate, although rf guns for producing nonpolarized electrons have not

yet performed at a level that is obviously better than the standard systems that have separate gun, bunching, and accelerating systems.

To operate rf guns with GaAs cathodes, the vacuum in the gun cavity with the rf on must be improved. In addition, there are at least three poorly known properties that must be determined.

- First, the time response of photoemitted electrons from GaAs must be very fast (on the order of tens of picoseconds or less).
- Second, the charge limit for photoemission, especially in the regime of very short pulses, must be high.
- Third, the effect of the rf wall currents on GaAs are yet to be determined.

On the other hand, research with new materials may some day result in a photocathode capable of producing high polarization that avoids some of the problems associated with GaAs [13].

A *hybrid gun*—a compromise between an rf gun and the traditional injector system—might consist of a very high voltage (pulsed) gun closely coupled to the first rf accelerating section. If the first few accelerating cavities have separate rf phase and amplitude controls, i.e., a buncher, then a relatively long gun pulse can be used. The longer pulse reduces the cathode requirements for fast time response and high charge limit. A very high gun voltage and physically close coupling would be necessary to minimize the space charge effects. The vacuum at the cathode would be expected to be somewhat better for this configuration. In addition, some means to divert most of the backward accelerated ions may be found. Since the accelerator in this case can be designed for traveling wave rf, the rf

duty factor can be significantly lower than for a conventional rf gun utilizing standing wave rf, thus reducing the dark current due to rf.

Conventional guns with more elaborate subharmonic bunching systems consisting of two or more rf cavities, each at progressively higher frequencies, are capable of producing high intensity beams with lower emittances. These systems are well understood, and represent the assured solution for improving injectors for the next generation of linacs.

Finally, mention should be made of the possiblity of generating flat beams with a photocathode source by using a laser beam with a flat cross section [14]. Such a technique may prove useful if, at the same time, the emittance can be made low enough to eliminate the damping ring. The solenoidal focusing used in most source designs, including rf guns, represents a complication for flat beams.

Acknowledgements

The author wishes to acknowledge useful conversations with D. Burke, R. Schindler, and others at SLAC.

References

[1] Most of the material of this section can be found in greater detail in refs. [2] and [3].

[2] C. Ahn et al., "Opportunities and Requirements for Experimentation at a Very High Energy e^+e^- Collider," SLAC–329 (1988).

[3] M.E. Peskin, "Physics Issues for the Next Linear Collider", in Physics and Experiments with Linear Colliders, R. Orava et al., eds., (Singapore: World Scientific, 1992) v. 1, p. 1.

[4] "JLC-I," KEK Report 92–16 (1992).

[5] D. Schultz et al., "Polarized Source Performance in 1992 for SLC–SLD," SLAC–PUB–6060 (1993), presented at the 10th Int. Sym. on High Energy Spin Physics, Nagoya, Nov 9–14, 1992.

[6] Most of the material of this section can be found in greater detail in M. L. Swartz, "Physics with Polarized Electron Beams," in Looking beyound the Z, Proc. Summer Institute on Particle Physics, E. C. Brennan, ed., Aug 1987, SLAC–328 (1988) p. 83.

[7] J.E. Clendenin et al., in XVth Int. Conf. on High Energy Accelerators, Int. J. Mod. Phys. A (Proc. Suppl.) 2A (1993) p. 151.

[8] T. Maruyama et al., Phys. Rev. B46 (1992) 4261; H. Aoyagi et al., Phys. Lett. A167 (1992) 415.

[9] M. Woods et al, "Observation of a Charge Limit for Semiconductor Photocathodes," SLAC–PUB–5894 (1992), to be published in J. Appl. Phys.; H. Tang et al., "Study of Non-Linear Photoemission Effects in III–V Semiconductors," SLAC–PUB–6167 (1993), presented at the 1993 Part. Acc. Conf., Washington, D.C.

[10] D. Schultz et al., "The High Peak Current Polarized Electron Source of the Stanford Linear Collider," these proceedings.

[11] R. E. Kirby et al., "An In-Situ Photocathode Loading System for the SLC Polarized Electron Gun," SLAC–PUB–6006 (1993), presented at the 1993 Part. Acc. Conf., Washington, D.C.

[12] J. Clendenin et al., "Prospects for Generating Polarized Electron Beams for a Linear Collider Using an rf Gun," these proceedings.

[13] For example, see V. L. Alperovich et al., "InGaAsP as a Promising Material for a Polarized Electron Source," presented at the 10th Int. Sym. on High Energy Spin Physics, Nagoya, Nov 9–14, 1992.

[14] J.B. Rosenzweig, "Asymmetric Emittance rf Photocathode Source for Linear Collider Applications," in Workshop on Fourth Generation Light Sources, SSRL Report 92/02 (1992) p. 253.

Table 1

Polarization asymmetries for e^+e^- reactions.

	A_{pol}
Standard model	
$e^+e^- \rightarrow u\bar{u}$	0.34
$e^+e^- \rightarrow d\bar{d}$	0.62
$e^+e^- \rightarrow W^+W^-$	0.94
$e^+e^- \rightarrow Z^\circ Z^\circ$	0.32
Superpartners	
$e^+e^- \rightarrow \tilde{u}_L \bar{\tilde{u}}_L$	0.94
$e^+e^- \rightarrow \tilde{u}_R \bar{\tilde{u}}_R$	−0.60
Higgs physics	
$e^+e^- \rightarrow \nu\bar{\nu} H^\circ$	1.00
$e^+e^- \rightarrow H^+H^-$	0.65

Figure Captions

1. Center-of-mass energy of constituents versus date of accelerator initial operation.
2. Schematic of a possible NLC design.
3. Differential cross sections for $e^+e^- \rightarrow W^+W^-$ in the SM at $\sqrt{s} = 1$ TeV as a function of the production angle ϑ, computed for left-handed (solid lines) and right-handed (dotted lines) polarized e^- on unpolarized e^+. The contributions from transverse and longitudinal W bosons are indicated by T and L respectively.
4. The expected error on Δm_W from the measurement of the beam polarization asymmetry as a function of the number of detected Z°s [4]. Each curve represents a different error on the beam polarization.
5. Differential cross sections for $e^+e^- \rightarrow t\bar{t}$ as a function of the production angle ϑ, computed for left-handed polarized e^-. The contributions from right- and left-handed top quarks are indicated by R and L respectively.
6. Feynman diagrams for two possible reactions that could produce H° in high energy e^+e^- collisions.
7. The mass of the standard model Higgs as a function of the W mass for various top masses [4].
8. The 1-σ contours in the m_t-m_H plane showing how the Higgs mass bound improves with the error on m_t [4].

9. Sketch of the SLC emphasizing the polarized electron beam components.
10. Polarimetry at the SLC.
11. Feynman diagrams for MØller scattering.
12. The unpolarized differential cross section for MØller scattering as a function of the center-of-mass angle. The longitudinal and transverse asymmetry functions are also shown.
13. A schematic of the SLC MØller polarimeter.
14. Feynman diagrams for Compton scattering.
15. The unpolarized cross section and the longitudinal and transverse polarization asymmetries as a function of x for the scattering of 2.23 eV photons by 46 GeV electrons.
16. A schematic diagram of a generic Compton polarimeter.

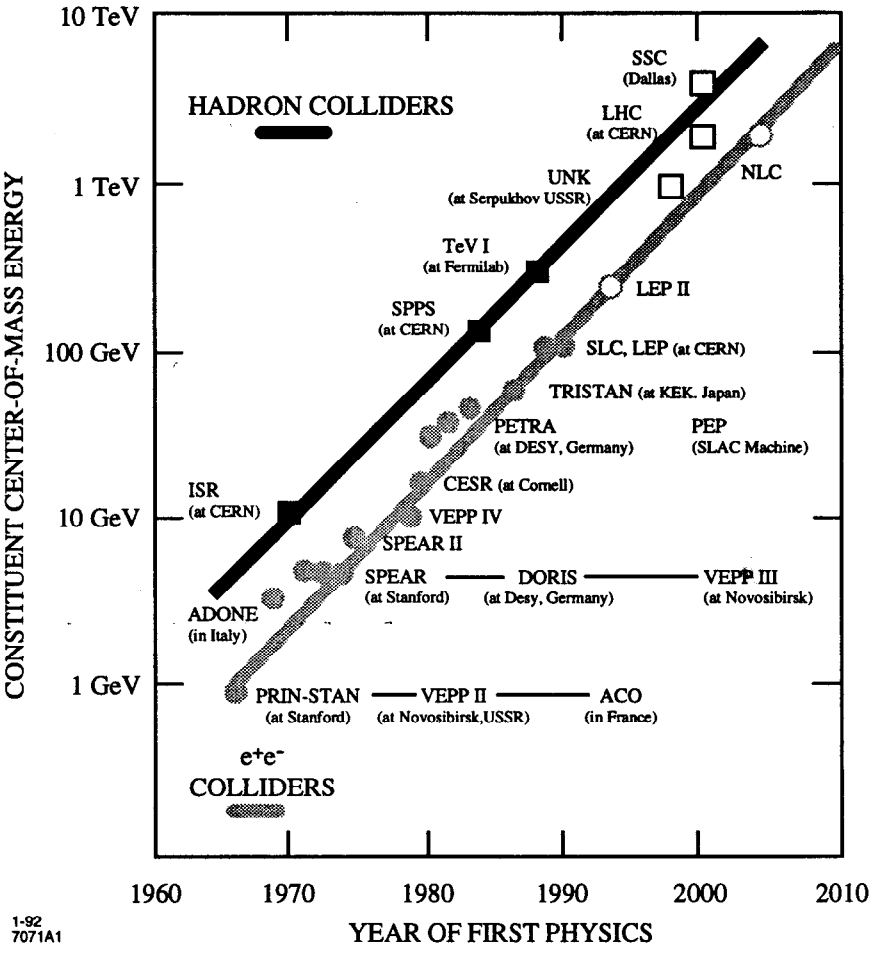
10 TeV
1 TeV
100 GeV
10 GeV
1 GeV
CONSTITUENT CENTER-OF-MASS ENERGY
HADRON COLLIDERS
SSC
(Dallas)
LHC
(at CERN)
UNK
(at Serpukhov USSR)
NLC
TeV I
(at Fermilab)
LEP II
SPPS
(at CERN)
SLC, LEP (at CERN)
TRISTAN (at KEK. Japan)
PETRA
(at DESY, Germany)
PEP
(SLAC Machine)
ISR
(at CERN)
CESR (at Cornell)
VEPP IV
SPEAR II
SPEAR
(at Stanford)
DORIS
(at Desy, Germany)
VEPP III
(at Novosibirsk)
ADONE
(in Italy)
PRIN-STAN
(at Stanford)
VEPP II
(at Novosibirsk,USSR)
ACO
(in France)
e+e-
COLLIDERS
1960
1970
1980
1990
2000
2010
YEAR OF FIRST PHYSICS
1-92
7071A1

Fig. 1

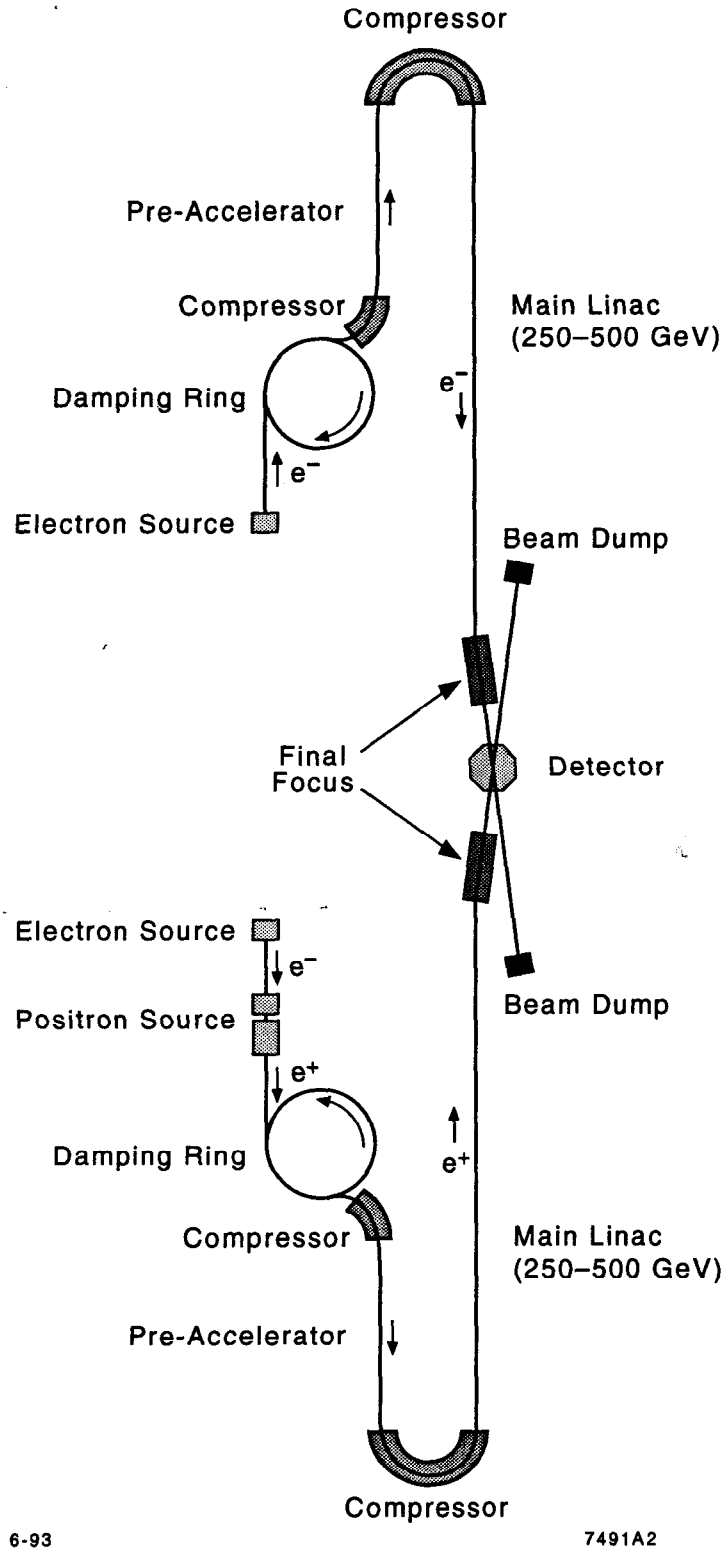
Compressor
Pre-Accelerator
Compressor
Main Linac
(250–500 GeV)
Damping Ring
e⁻
e⁻
Electron Source
Beam Dump
Final
Focus
Detector
Electron Source
e⁻
Positron Source
e⁺
Beam Dump
Damping Ring
e⁺
Compressor
Main Linac
(250–500 GeV)
Pre-Accelerator
Compressor
6-93
7491A2

Fig. 2

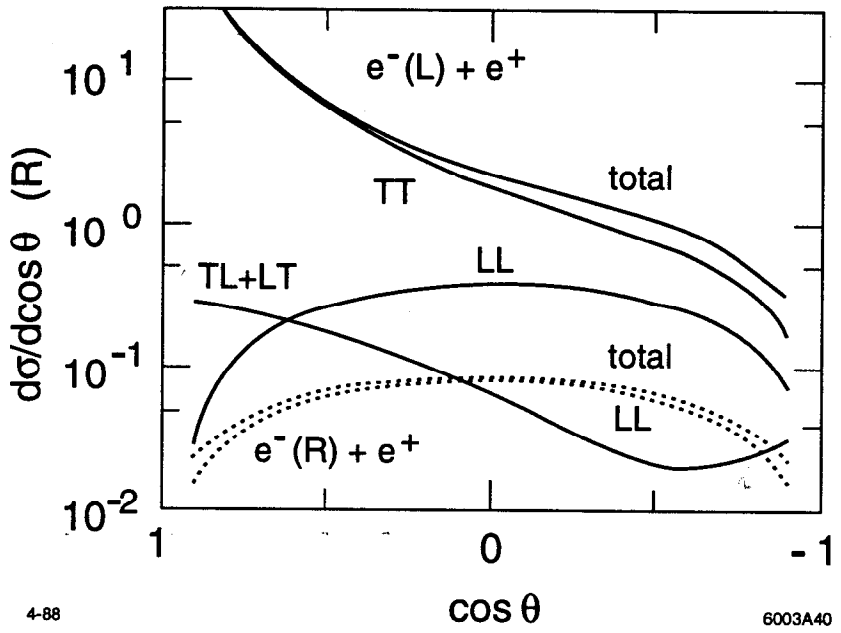
10^1
10^0
10^{-1}
10^{-2}
$d\sigma/d\cos\theta$ (R)
$e^-(L) + e^+$
TT
total
TL+LT
LL
total
LL
$e^-(R) + e^+$
1
0
- 1
cos θ
4-88
6003A40

Fig. 3

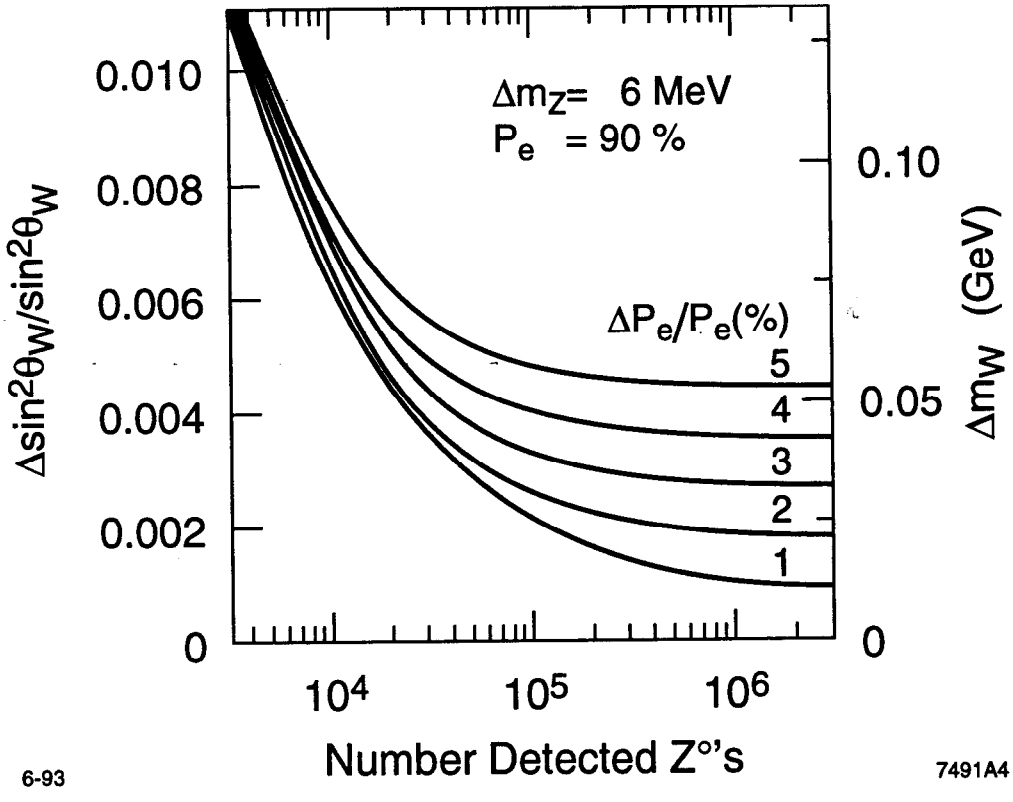
0.010
0.008
0.006
0.004
0.002
0
$\Delta\sin^2\theta_W/\sin^2\theta_W$
Δm_Z= 6 MeV
P_e = 90 %
$\Delta P_e/P_e$(%)
5
4
3
2
1
0.10
0.05
0
Δm_W (GeV)
10^4
10^5
10^6
Number Detected Z°'s
6-93
7491A4

Fig. 4

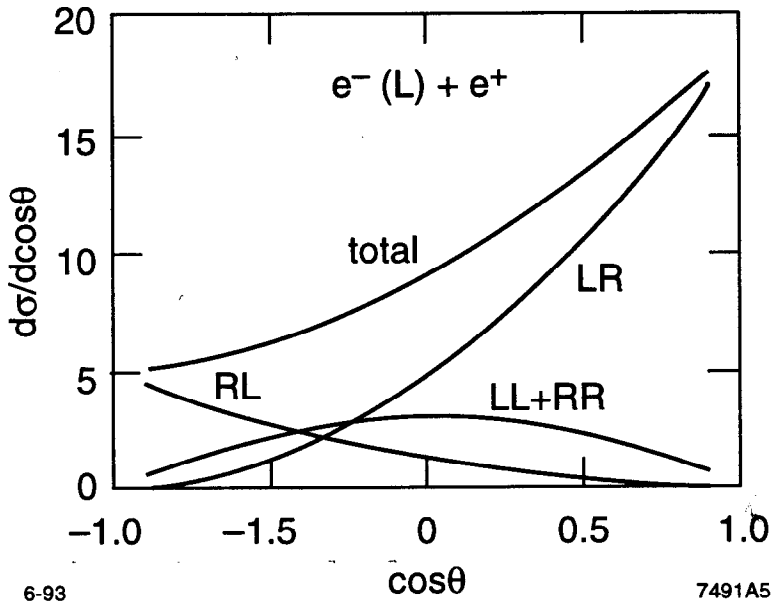
20
15
10
5
0
dσ/dcosθ
e⁻ (L) + e⁺
total
LR
RL
LL+RR
−1.0
−1.5
0
0.5
1.0
cosθ
6-93
7491A5

Fig. 5

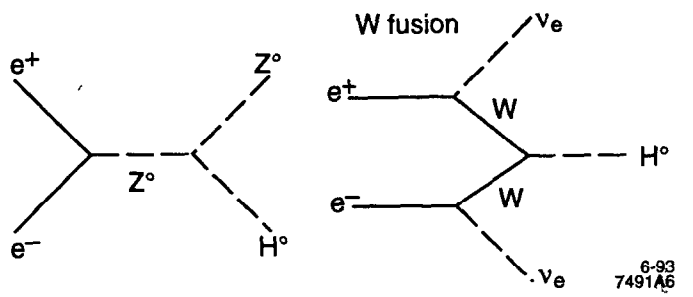

Fig. 6

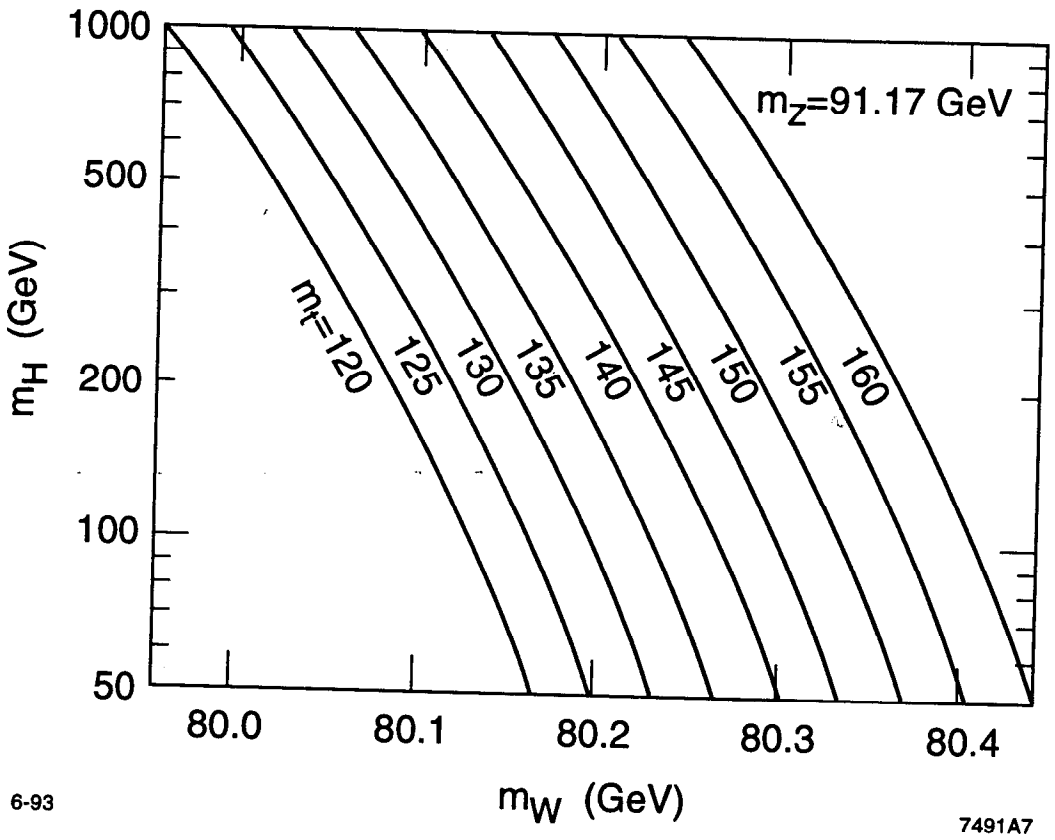
1000
500
200
100
50
m_H (GeV)
m_Z=91.17 GeV
m_t=120
125
130
135
140
145
150
155
160
80.0
80.1
80.2
80.3
80.4
m_W (GeV)
6-93
7491A7

Fig. 7

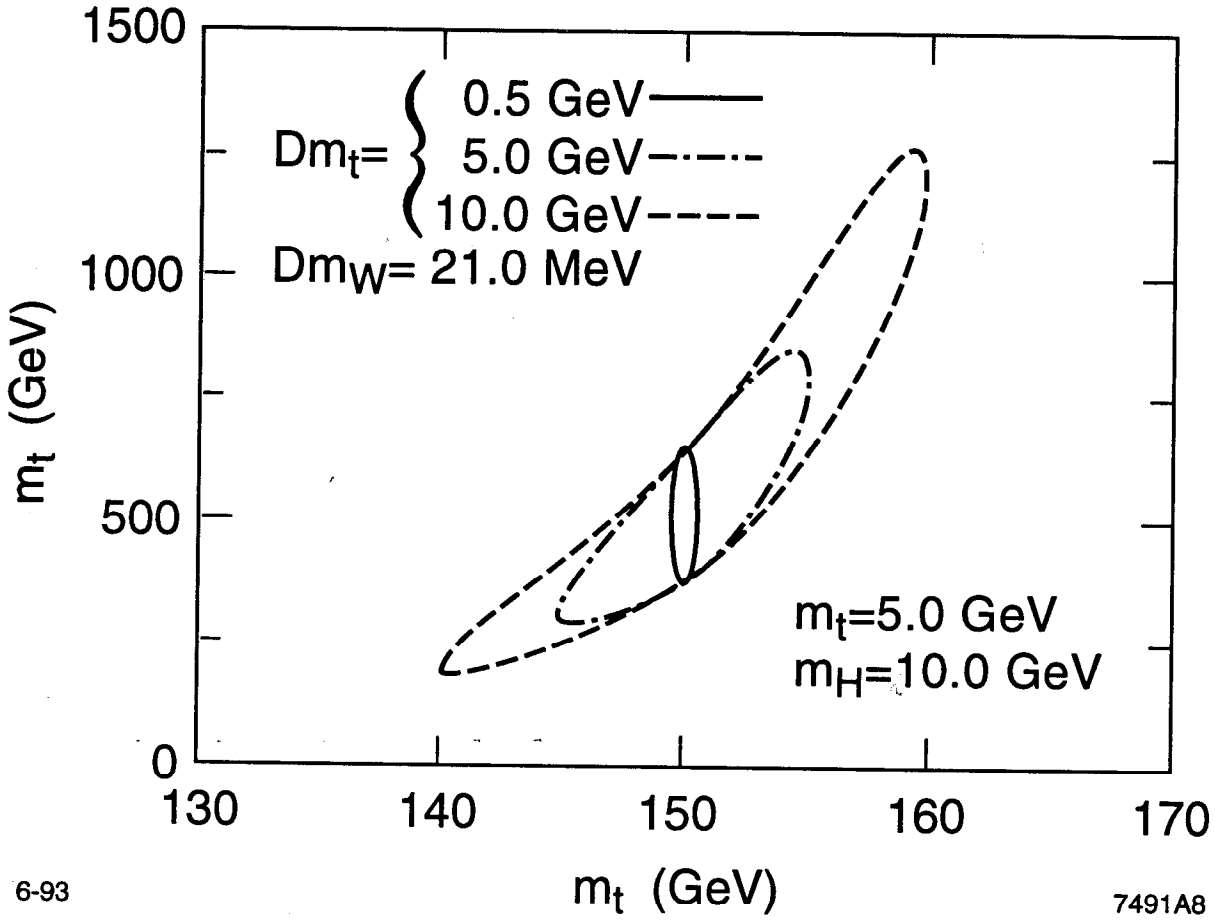
1500
1000
500
0
130
140
150
160
170
m_t (GeV)
m_t (GeV)
Dm_t= 0.5 GeV
5.0 GeV
10.0 GeV
Dm_W= 21.0 MeV
m_t=5.0 GeV
m_H=10.0 GeV
6-93
7491A8

Fig. 8

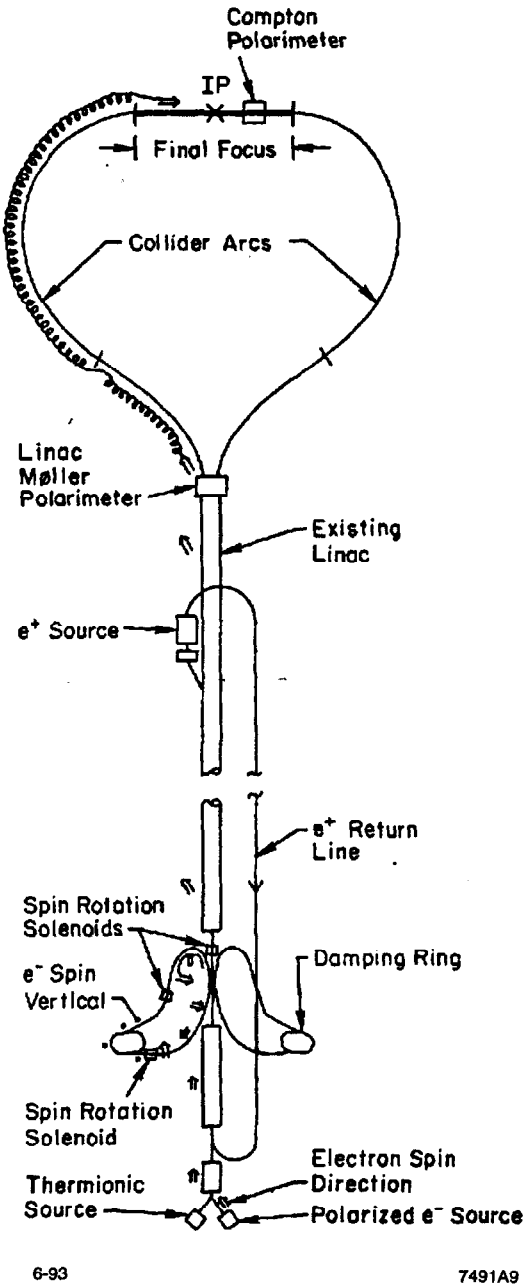
Compton
Polarimeter
IP
Final Focus
Collider Arcs
Linac
Møller
Polarimeter
Existing
Linac
e+ Source
e+ Return
Line
Spin Rotation
Solenoids
e- Spin
Vertical
Damping Ring
Spin Rotation
Solenoid
Electron Spin
Direction
Thermionic
Source
Polarized e- Source
6-93
7491A9

Fig. 9

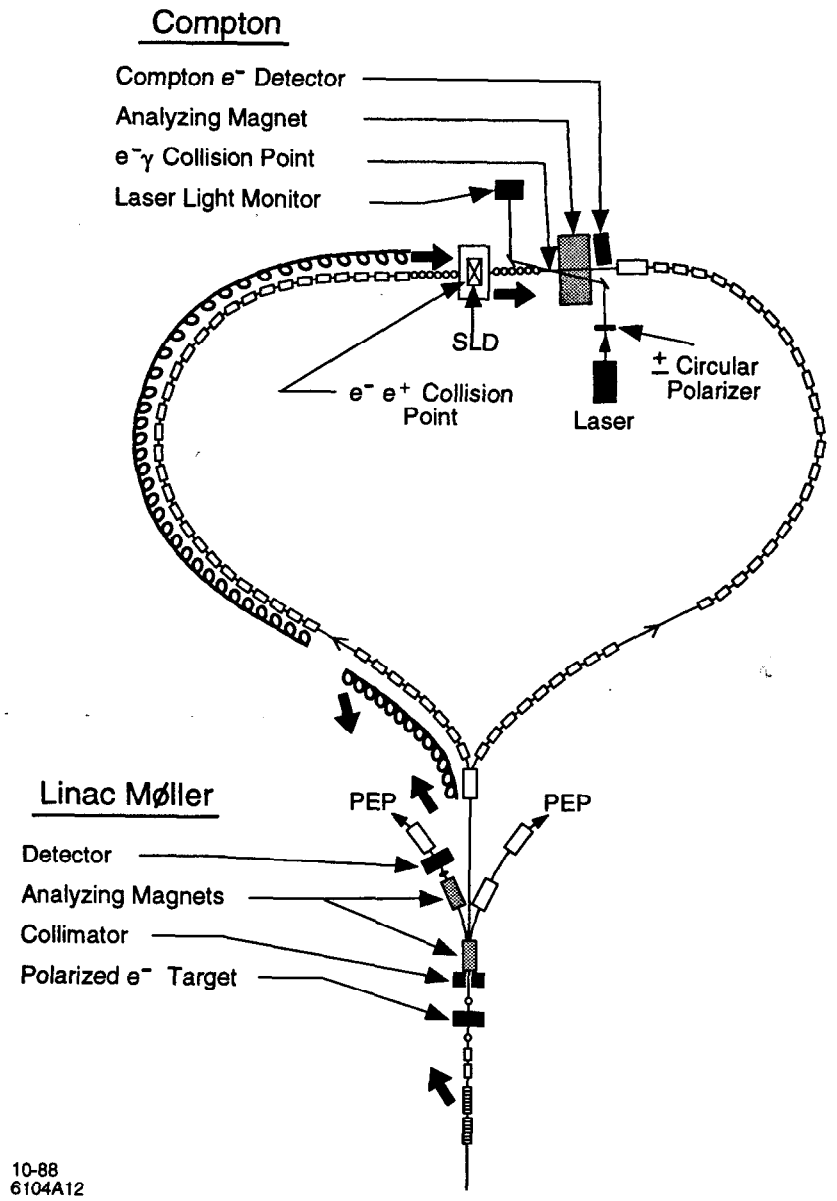
Compton
Compton e⁻ Detector
Analyzing Magnet
e⁻γ Collision Point
Laser Light Monitor
SLD
e⁻ e⁺ Collision Point
± Circular Polarizer
Laser
Linac Møller
PEP
PEP
Detector
Analyzing Magnets
Collimator
Polarized e⁻ Target
10-88
6104A12

Fig. 10

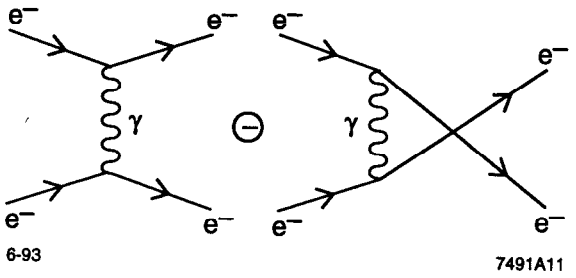

Fig. 11

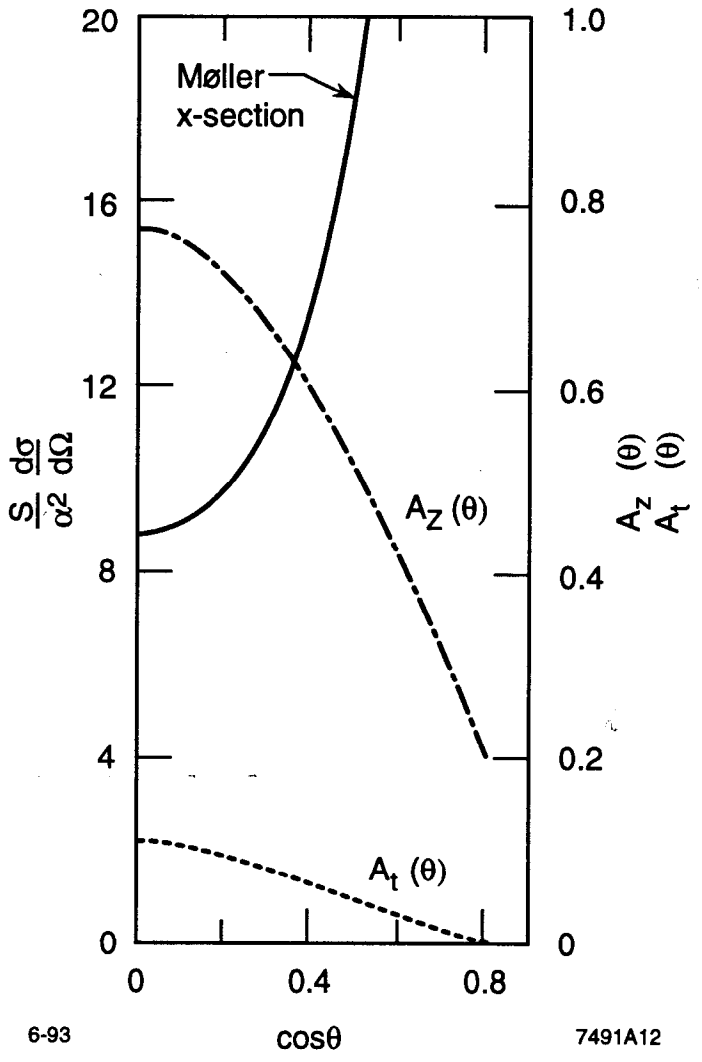
20
16
12
8
4
0
1.0
0.8
0.6
0.4
0.2
0
0
0.4
0.8
Møller
x-section
A_Z (θ)
A_t (θ)
$\frac{S}{\alpha^2}\frac{d\sigma}{d\Omega}$
A_Z (θ)
A_t (θ)
cosθ
6-93
7491A12

Fig. 12

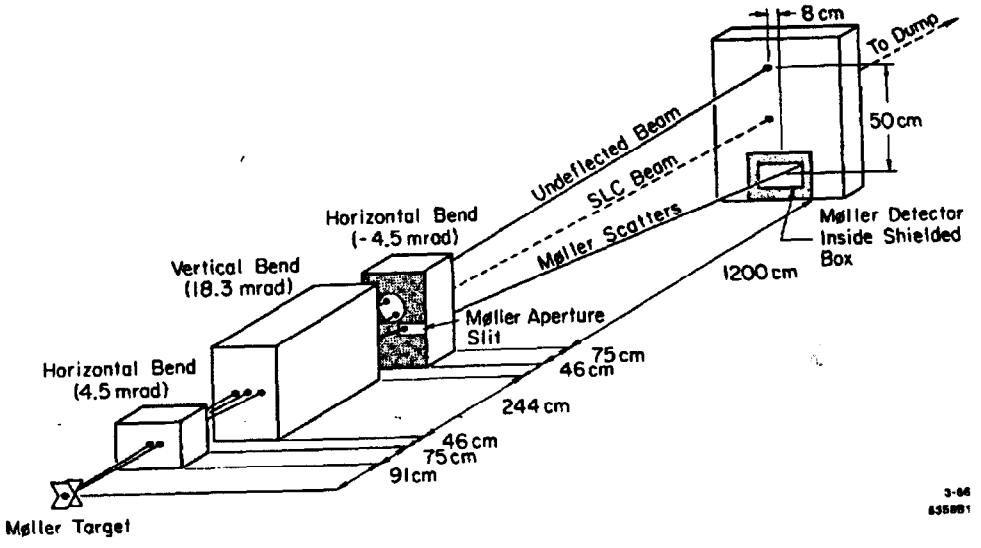
8 cm
To Dump
50 cm
Undeflected Beam
SLC Beam
Møller Scatters
Horizontal Bend
(-4.5 mrad)
Vertical Bend
(18.3 mrad)
Møller Aperture
Slit
Horizontal Bend
(4.5 mrad)
75 cm
46 cm
244 cm
46 cm
75 cm
91 cm
Møller Target
1200 cm
Møller Detector
Inside Shielded
Box

Fig. 13

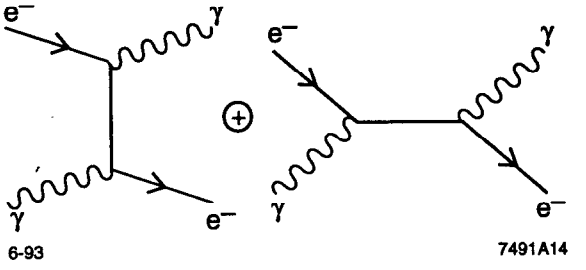

Fig. 14

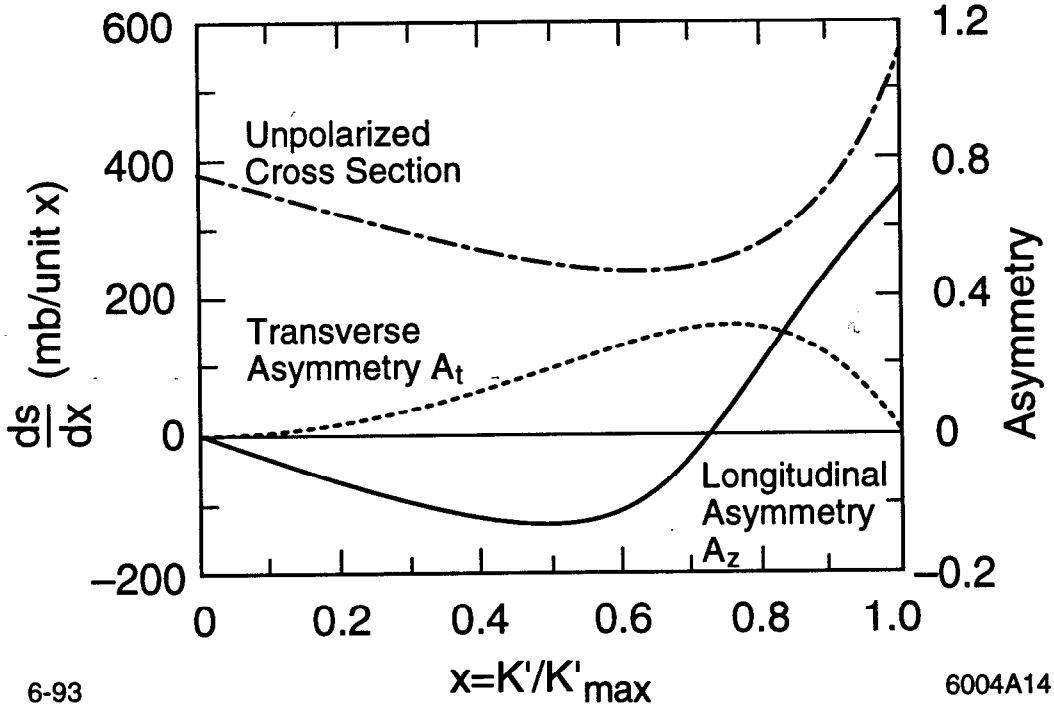
600
400
200
0
–200
1.2
0.8
0.4
0
–0.2
Asymmetry
ds/dx (mb/unit x)
Unpolarized
Cross Section
Transverse
Asymmetry A_t
Longitudinal
Asymmetry
A_z
0
0.2
0.4
0.6
0.8
1.0
x=K'/K'max
6-93
6004A14

Fig. 15

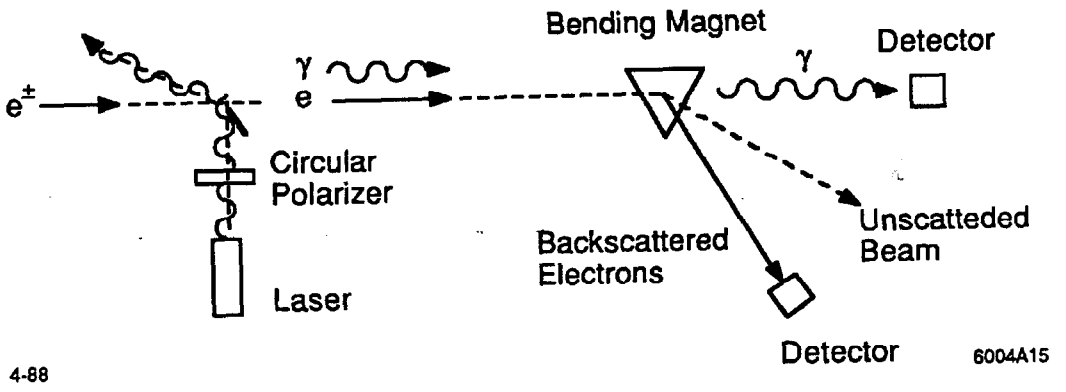
Bending Magnet
Detector
γ
e±
γ
e
Circular
Polarizer
Laser
Unscatteded
Beam
Backscattered
Electrons
Detector
4-88
6004A15

Fig. 16